Available online at www.sciencedirect.com
ScienceDirect
Journal of Sound and Vibration 319 (2009) 940–962
JOURNAL OF SOUND AND VIBRATION
www.elsevier.com/locate/jsvi

Numerical analysis of isolation of the vibration due to moving loads using pile rows

Jian-Fei Lu[a,*], Bin Xu[b], Jian-Hua Wang[b]

[a]Department of Civil Engineering, Jiangsu University, Zhenjiang, Jiangsu 212013, PR China
[b]Department of Civil Engineering, Shanghai JiaoTong University, Shanghai 200030, PR China

Received 13 February 2008; received in revised form 17 June 2008; accepted 21 June 2008
Handling Editor: L.G. Tham
Available online 3 August 2008

Abstract

The isolation of the vibration due to moving loads using pile rows embedded in a poroelastic half-space is investigated in this study. Based on Biot's theory and integral transform method, the free field solution for a moving load applied on the surface of a poroelastic half-space and the fundamental solution for a harmonic circular patch load applied in the poroelastic half-space are derived first. Using Muki and Sternberg's method and the fundamental solution for the circular patch load as well as the obtained free field solution for the moving load, the second kind of Fredholm integral equations in the frequency domain describing the dynamic interaction between pile rows and the poroelastic half-space is developed. Numerical solution of the frequency domain integral equations and numerical inversion of the Fourier transform yield the time domain response of the pile–soil system. Comparison of our results with some known results shows that our results are in a good agreement with existing ones. Numerical results of this study show that velocity of moving loads has an important impact on the vibration isolation effect of pile rows. The same pile row has a better vibration isolation effect for the lower speed moving loads than for the higher speed ones. Also, the optimal length of piles for higher speed moving loads is shorter than that for lower speed moving loads. Moreover, stiff pile rows tend to produce a better vibration isolation effect than flexible pile rows do.

1. Introduction

Vibration induced by railway traffic is a major concern for civil engineers as it can cause annoyance to residents or even damage to adjacent structures. Generally, the effects of ground vibrations can be mitigated by two kinds of vibration isolation methods: the active and the passive vibration isolation method. The active isolation system is often used to isolate the vibration source from the ground and thus, it is usually installed around the vibration source in a very close distance. The passive isolation system, on the other hand, is often used to reduce the energy transported to structures and consequently, it usually surrounds the protected structure.

Roughly, there are two passive vibration isolation methods: the trench (open or unfilled) isolation method and the pile (pile rows or sheet piles) isolation method. To date, many researches concerning vibration isolation by trenches or piles have been conducted. For example, Emad and Manolis [1] utilized the boundary

*Corresponding author. Tel. +86 51188791011.
E-mail addresses: ljfdoctor@yahoo.com (J.-F. Lu), xubin1@sjtu.edu.cn (B. Xu), wjh417@sjtu.edu.cn (J.-H. Wang).

0022-460X/$ - see front matter © 2008 Elsevier Ltd. All rights reserved.
doi:10.1016/j.jsv.2008.06.032

element method (BEM) with constant elements to examine the efficiency of vibration reduction by open trench with a rectangular or a circular cross-section. Beskos et al. [2] employed BEM with constant elements to investigate the effect of the vibration reduction using open and infilled trenches. Dasgupta et al. [3] applied three-dimensional (3-D) frequency domain BEM with the full space fundamental solution to analyze the isolation of the vibration due to a rigid surface foundation subjected to harmonic loading by open and infilled trenches. Avilles and Sanchez-Sesma [4] developed theoretical models to study the vibration reduction effect behind a pile row when subjected to the SV wave and the Rayleigh wave. Kattis et al. [5,6] used the 3-D frequency domain BEM to calculate the screening effectiveness of a pile row. Also, by means of the frequency domain BEM, the screening effectiveness of four types of circular piles in a row against the vibration due to a massless square foundation subjected to a harmonic vertical loading is studied by Tsai [7].

It should be noticed that previous researches concerning the vibration isolation in a half-space unanimously treat the half-space as a single-phase elastic medium. Nevertheless, in many areas of southeast China, the earth's surface is covered by saturated soil. This is especially the case in Shanghai where a high-speed railway is being established on the fluid-saturated porous soil. It is well known that for saturated soil, the pore fluid plays a crucial role in the liquefaction and the shear failure of the soil. Thus, it is insufficient to treat the saturated soil as a single-phase elastic medium. However, to date, for the vibration isolation problem in a saturated poroelastic medium, no research has been carried out. To the knowledge of the authors, all the existing researches concerning the dynamic response of pile embedded in a poroelastic half-space are limited to the case of piles subjected to top harmonic loads. For example, based on Biot's theory [8–10], Zeng and Rajapakse [11] analyzed the steady-state dynamic response of an axially loaded elastic pile embedded in a poroelastic half-space. Wang et al. [12] extended the problem to dynamic response of pile groups embedded in a poroelastic half-space. More recently, Jin et al. [13] studied the time-harmonic response of a pile under lateral loadings in a poroelastic half-space.

In this paper, a numerical method for evaluating the vibration isolation effect of pile rows embedded in a poroelastic half-space subjected to a vertical moving load is developed on the basis of Biot's theory and Muki and Sternberg's method [14,15]. Based on the proposed method, the influence of various parameters on the vibration isolation effect of pile rows embedded in the poroelastic half-space is investigated numerically. It is worth noting that the proposed approach in this study belongs to the semi-analytical category. Thus, compared with the conventional domain discretization methods such as finite element method and BEM, it can reduce CPU time significantly for the current full 3-D time-consuming problem.

2. The free wave field solution and the fundamental solution for a circular uniform patch load

2.1. Biot's theory

In this study, the soil is considered as a half-space poroelastic medium, which is described by Biot's theory [8–10]. Equations of motion for the bulk material and the pore fluid of the porous medium are expressed in terms of the solid displacement (u_i) and the infiltration displacement (w_i) as follows [8–10]:

$$\mu u_{i,jj} + (\lambda + \alpha^2 M + \mu) u_{j,ji} + \alpha M w_{j,ji} = \rho \ddot{u}_i + \rho_f \ddot{w}_i \tag{1a}$$

$$\alpha M u_{j,ji} + M w_{j,ji} = \rho_f \ddot{u}_i + m \ddot{w}_i + b_p \dot{w}_i \tag{1b}$$

where λ and μ are Lame constants of the solid skeleton, ρ is the bulk density of the porous medium, which is equal to $\rho = (1-\phi)\rho_s + \phi\rho_f$ (where ρ_s is the density of the solid skeleton and ρ_f is the density of the pore fluid), ϕ is the porosity of the poroelastic medium, $m = a_\infty \rho_f / \phi$ and a_∞ is the tortuosity of the porous medium; $b_p = \eta/k$, η and k represent the viscosity of the pore fluid and the permeability of the porous medium, respectively, the superimposed dot above a variable denotes the time derivative.

According to Biot's theory, constitutive relations for a homogeneous porous medium have the form [10]

$$\sigma_{ij} = 2\mu\varepsilon_{ij} + \lambda\delta_{ij} e - \alpha\delta_{ij} p_f \tag{2a}$$

$$p_f = -\alpha M e + M\vartheta \tag{2b}$$

where σ_{ij} is the stress of bulk material, ε_{ij} denotes the strain tensor of the solid skeleton, p_f is the excess pore fluid pressure and δ_{ij} is the Kronecker delta. In Eq. (2b), the dilatation of the solid skeleton e and fluid volume increment ϑ are defined as

$$e = u_{i,i}, \quad \vartheta = -w_{i,i} \tag{3}$$

2.2. Free wave field solution due to the moving loads

In this study, the free wave field solution is defined as the solution of the moving load in the absence of the pile rows. To establish Fredholm integral equations describing the dynamic interaction between the piles and the half-space under moving loads, the free field solution for the moving load is required in advance.

For a moving load, axisymmetry is lost due to the orientation of the motion of the load. Thus, it is more convenient to consider the moving load problem in a Cartesian coordinate system. To derive the general solutions for Biot's equations in the frequency domain, the Fourier transform with respect to time and frequency is involved [16], which is defined as follows:

$$\bar{f}(\omega) = \int_{-\infty}^{+\infty} f(t)\mathrm{e}^{-\mathrm{i}\omega t}\,\mathrm{d}t, \quad f(t) = \frac{1}{2\pi}\int_{-\infty}^{+\infty} \bar{f}(\omega)\mathrm{e}^{-\mathrm{i}\omega t}\,\mathrm{d}\omega \tag{4}$$

where $f(t)$ represents a function in the time domain, $\bar{f}(\omega)$ is the Fourier transform of $f(t)$, t and ω denote time and frequency, respectively.

In the frequency domain, the governing equations of Biot's theory can be reduced to three Helmholtz equations for the scalar ($\bar{\varphi}_f$, $\bar{\varphi}_s$) and the vector potential ($\bar{\boldsymbol{\psi}}$) corresponding to the P1 wave, the P2 wave and the S wave of the porous medium as follows:

$$\nabla^2\bar{\varphi}_f + k_f^2\bar{\varphi}_f = 0 \tag{5a}$$

$$\nabla^2\bar{\varphi}_s + k_s^2\bar{\varphi}_s = 0 \tag{5b}$$

$$\nabla^2\bar{\boldsymbol{\psi}} + k_t^2\bar{\boldsymbol{\psi}} = 0 \tag{5c}$$

where the vector potential ($\bar{\boldsymbol{\psi}}$) satisfy $\hat{\psi}_{i,i} = 0$ and the complex wavenumber k_f, k_s, k_t are given by

$$k_f^2 = (\beta_4 A_f - \beta_3)/A_f, \quad k_s^2 = (\beta_4 A_s - \beta_3)/A_s, \quad k_t^2 = \beta_2/\mu \tag{6}$$

in which $\beta_1 = \alpha - \rho_f\omega^2/\beta_5$, $\beta_2 = \rho\omega^2 - \rho_f^2\omega^4/\beta_5$, $\beta_3 = \rho_f\omega^2 - \alpha\beta_5$, $\beta_4 = \beta_5/M$, $\beta_5 = m\omega^2 - \mathrm{i}b_p\omega$. In Eq. (6), A_f and A_s are two constants given by

$$A_{f,s}^2 + \frac{\beta_2 - (\lambda+2\mu)\beta_4 - \beta_1\beta_3}{\beta_1\beta_4}A_{f,s} + \frac{(\lambda+2\mu)\beta_3}{\beta_1\beta_4} = 0 \tag{7}$$

The displacement and the pore pressure of the porous medium can be further represented by

$$\bar{u}_i = \bar{\varphi}_{f,i} + \bar{\varphi}_{s,i} + \mathrm{e}_{ijk}\bar{\psi}_{k,j} \tag{8a}$$

$$\bar{p}_f = A_f\bar{\varphi}_{f,ii} + A_s\bar{\varphi}_{s,ii} \tag{8b}$$

The general solutions for the potentials can be derived through the Fourier transform with respect to the horizontal coordinates. The Fourier transform for the two horizontal coordinates are defined as follows [16]:

$$\hat{f}(k_x) = \int_{-\infty}^{+\infty} f(x)\mathrm{e}^{-\mathrm{i}k_x x}\,\mathrm{d}x, \quad f(x) = \frac{1}{2\pi}\int_{-\infty}^{+\infty} \hat{f}(k_x)\mathrm{e}^{\mathrm{i}k_x x}\,\mathrm{d}k_x \tag{9}$$

$$\tilde{f}(k_y) = \int_{-\infty}^{+\infty} f(y)\mathrm{e}^{-\mathrm{i}k_y y}\,\mathrm{d}y, \quad f(y) = \frac{1}{2\pi}\int_{-\infty}^{+\infty} \tilde{f}(k_y)\mathrm{e}^{\mathrm{i}k_y y}\,\mathrm{d}k_y \tag{10}$$

where k_x, k_y represent the two horizontal wavenumbers corresponding to x- and y-coordinates, respectively.

Once the potentials for the half-space porous medium ($\tilde{\tilde{\varphi}}_f, \tilde{\tilde{\varphi}}_s$ and $\tilde{\tilde{\psi}}_i$) are determined, the frequency wavenumber domain displacement ($\tilde{\tilde{u}}_z$), the stresses ($\tilde{\tilde{\sigma}}_{zz}, \tilde{\tilde{\sigma}}_{zx}$ and $\tilde{\tilde{\sigma}}_{zy}$) and the pore pressure ($\tilde{\tilde{p}}_f$) have the following expressions [17]:

$$\begin{aligned}
\tilde{\tilde{u}}_z(k_x,k_y,z,\omega) = & -B(k_x,k_y,\omega)\gamma_t e^{-\gamma_t z} - D(k_x,k_y,\omega)\gamma_s e^{-\gamma_s z} \\
& - \mathrm{i}[k_y F(k_x,k_y,\omega) - k_x H(k_x,k_y,\omega)]e^{-\gamma_t z} \\
\tilde{\tilde{\sigma}}_{zz}(k_x,k_y,z,\omega) = & -(\lambda-2\mu)[B(k_x,k_y,\omega)k_f^2 e^{-\gamma_f z} + D(k_x,k_y,\omega)k_s^2 e^{-\gamma_s z}] \\
& - 2\mu\mathrm{i}[\eta F(k_x,k_y,\omega)\gamma_t e^{-\gamma_t z} - H(k_x,k_y,\omega)\gamma_t k_x e^{-\gamma_t z}] - \alpha\tilde{\tilde{p}}_f \\
\tilde{\tilde{\sigma}}_{zx}(k_x,k_y,z,\omega) = & \mu[2\mathrm{i}k_x\gamma_f B(k_x,k_y,\omega)e^{-\gamma_f z} - 2\mathrm{i}k_x\gamma_s D(k_x,k_y,\omega)e^{-\gamma_s z} \\
& + 2k_x k_y F(k_x,k_y,\omega)e^{-\gamma_t z} + (k_y^2 - k_x^2 - \gamma_t^2)H(k_x,k_y,\omega)e^{-\gamma_t z}] \\
\tilde{\tilde{\sigma}}_{zy}(k_x,k_y,z,\omega) = & \mu[-2\mathrm{i}k_x\gamma_f B(k_x,k_y,\omega)e^{-\gamma_f z} - 2\mathrm{i}k_y\gamma_s D(k_x,k_y,\omega)e^{-\gamma_s z} \\
& + (k_y^2 + k_x^2 + \gamma_t^2)F(k_x,k_y,\omega)e^{-\gamma_t z} - 2k_x k_y H(k_x,k_y,\omega)e^{-\gamma_t z}] \\
\tilde{\tilde{p}}_f(k_x,k_y,z,\omega) = & -B(k_x,k_y,\omega)A_f k_f^2 e^{-\gamma_t z} - D(k_x,k_y,\omega)A_s k_s^2 e^{-\gamma_s z}
\end{aligned} \tag{11a - e}$$

where $B(k_x,k_y,\omega)$, $D(k_x,k_y,\omega)$, $F(k_x,k_y,\omega)$ and $H(k_x,k_y,\omega)$ are the arbitrary constants to be determined by the boundary conditions, and γ_f, γ_s, γ_t have the following expressions:

$$\gamma_f^2 = k_x^2 + k_y^2 - k_f^2, \quad \gamma_s^2 = k_x^2 + k_y^2 - k_s^2, \quad \gamma_t^2 = k_x^2 + k_y^2 - k_t^2 \tag{12}$$

in which roots of γ_f, γ_s, γ_t are chosen to satisfy $\mathrm{Re}(\gamma_f)\geqslant 0$, $\mathrm{Re}(\gamma_s)\geqslant 0$ and $\mathrm{Re}(\gamma_t)\geqslant 0$.

In this study, it is assumed that the moving load with a constant speed c and an oscillating frequency ω_0 (Fig. 1) is applied on the surface of the poroelastic half-space. The load moves along the positive direction of the y-axis and the distance between the trace of the load and the y-axis is d_s (Fig. 1). Also, the half-space surface is assumed to be completely permeable. For the moving load applied over a rectangular area $2a\times 2b$, the boundary conditions in the time–space domain are as follows:

$$\sigma_{zx}(x,y,z,t)\big|_{z=0} = 0 \tag{13a}$$

$$\sigma_{zy}(x,y,z,t)\big|_{z=0} = 0 \tag{13b}$$

$$p_f(x,y,z,t)\big|_{z=0} = 0 \tag{13c}$$

$$\begin{aligned}
\sigma_{zz}(x,y,z,t)\big|_{z=0} = & -q_z[H(x+d_s+a) - H(x+d_s-a)] \\
& \times [H(y-y_0+b-ct) - H(y-y_0-b-ct)]e^{\mathrm{i}\omega_0 t}
\end{aligned} \tag{13d}$$

where q_z is the intensity of the distributed load, ω_0 the frequency of the moving load, $H(*)$ the Heaviside step function and y_0 the y coordinate of the center of the distributed load at time $t=0$.

Performing a triple Fourier transform with respect to time and the two horizontal coordinates, respectively, on Eq. (13), we have the following boundary condition in the frequency wavenumber domain:

$$\tilde{\tilde{\sigma}}_{zx}(k_x,k_y,0,\omega) = 0 \tag{14a}$$

$$\tilde{\tilde{\sigma}}_{zy}(k_x,k_y,0,\omega) = 0 \tag{14b}$$

$$\tilde{\tilde{p}}_f(k_x,k_y,0,\omega) = 0 \tag{14c}$$

$$\tilde{\tilde{\sigma}}_{zz}(k_x,k_y,0,\omega) = -8\pi q_z \frac{\sin(k_x a)}{k_x}\frac{\sin(k_y b)}{k_y}e^{\mathrm{i}(k_x d_s - k_y y_0)}\delta(\omega-\omega_0+k_y c) \tag{14d}$$

where $\delta(*)$ is the Dirac delta function.

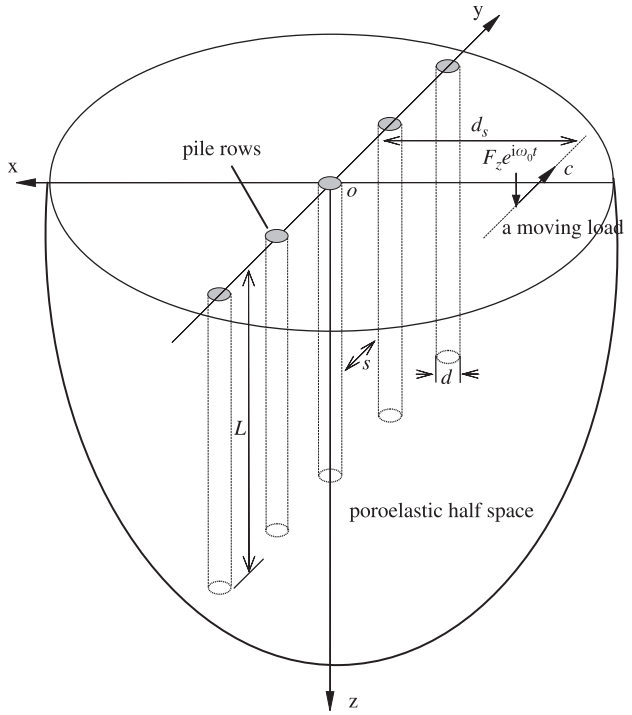

Fig. 1. Piles rows embedded in a poroelastic half-space to isolate the vibration due to a moving load.

For a moving point load, the boundary conditions for σ_{zx}, σ_{zy}, p_f are the same as those for the moving rectangular distributed load, while the boundary condition for σ_{zz} is as follows:

$$\sigma_{zz}(x,y,z,t)\big|_{z=0} = -F_z\delta(x+d_s)\delta(y-y_0-ct)\mathrm{e}^{\mathrm{i}\omega_0 t} \tag{15}$$

Likewise, the boundary condition for $\tilde{\tilde{\bar{\sigma}}}_{zz}$ in the frequency wavenumber domain is given by

$$\tilde{\tilde{\bar{\sigma}}}_{zz}(k_x,k_y,0,\omega) = -2\pi F_z\mathrm{e}^{\mathrm{i}(k_x d_s - k_y y_0)}\delta(\omega-\omega_0+ck_y) \tag{16}$$

Using Eqs. (11) and (14) or Eq. (16), the arbitrary constants $B(k_x,k_y,\omega)$, $D(k_x,k_y,\omega)$, $F(k_x,k_y,\omega)$ and $H(k_x,k_y,\omega)$ can be determined. After determining the arbitrary constants, the free wave field due to the surface moving load in the frequency wavenumber domain can be determined by Eq. (11). In view of Eq. (14), all the variables in the frequency wavenumber domain for the moving distributed rectangular load can be expressed in the following form:

$$\tilde{\tilde{\bar{\Omega}}}(k_x,k_y,z,\omega) = \left[-8\pi q_z\frac{\sin(k_x a)}{k_x}\frac{\sin(k_y b)}{k_y}\,\mathrm{e}^{\mathrm{i}(k_x d_s - k_y y_0)}\delta(\omega-\omega_0+k_y c)\right]\tilde{\tilde{\bar{\Omega}}}^*(k_x,k_y,z,\omega) \tag{17}$$

where $\tilde{\tilde{\bar{\Omega}}}^*(k_x,k_y,z,\omega)$ is the solution for a variable corresponding to a unit boundary value $\tilde{\tilde{\bar{\sigma}}}_{zz}$ in Eq. (14d). For the moving point load, we have the similar expression

$$\tilde{\tilde{\bar{\Omega}}}(k_x,k_y,z,\omega) = \left[-2\pi F_z\mathrm{e}^{\mathrm{i}(k_x d_s - k_y y_0)}\delta(\omega-\omega_0+ck_y)\right]\tilde{\tilde{\bar{\Omega}}}^*(k_x,k_y,z,\omega) \tag{18}$$

Performing the inverse Fourier transform with respect to the two horizontal wavenumbers and using the property of the delta function, the frequency domain free field solution for the moving distributed rectangular load has the form

$$\bar{\Omega}(x,y,z,\omega) = -\frac{2q_z}{\pi}\frac{\sin[b(\omega_0-\omega)/c]}{\omega_0-\omega}\mathrm{e}^{\mathrm{i}(\omega_0-\omega/c)(y-y_0)}\int_{-\infty}^{+\infty}\frac{\sin(k_x a)}{k_x}\,\hat{\bar{\Omega}}^*\left(k_x,\frac{\omega_0-\omega}{c},z,\omega\right)\mathrm{e}^{\mathrm{i}k_x(x+d_s)}\,\mathrm{d}k_x \tag{19}$$

For the moving point load, the frequency domain free field solution for all the variables is represented by

$$\bar{\Omega}(x,y,z,\omega) = -\frac{F_z}{2\pi c} e^{i(\omega_0-\omega)/c(y-y_0)} \int_{-\infty}^{+\infty} \hat{\bar{\Omega}}^* \left(k_x, \frac{\omega_0-\omega}{c}, z, \omega\right) e^{ik_x(x+d_s)}\, dk_x \tag{20}$$

2.3. The fundamental solution for a harmonic circular uniform patch load

To establish the integral equations for the pile rows, the frequency domain fundamental solution for a uniform vertical patch load applied in the poroelastic half-space is required. As the problem for a poroelastic half-space subjected to a uniform vertical patch load over a circular area with a radius R (Fig. 2) is axisymmetric with respect to the center of the circular area, thus, it is more convenient to consider the problem in the cylindrical coordinate system (r,θ,z).

In the cylindrical coordinate system (r,θ,z), the governing equations of Biot's theory can be reduced to Helmholtz equations for the scalar and the vector potential corresponding to the P1 wave, the P2 wave and the S wave of the porous medium. The Helmholtz equations for the scalar in the cylindrical coordinate system are the same as Eqs. (5a) and (5b), and the vector potential for the axisymmetric case can be reduced to a scalar potential $\bar{\eta}$, which fulfill the following Helmholtz equation:

$$\nabla^2\bar{\eta} + k_t^2\bar{\eta} = 0 \tag{21}$$

The displacement of the solid skeleton can be expressed by the potentials as follows:

$$\bar{u}_r = \frac{\partial\bar{\varphi}_f}{\partial r} + \frac{\partial\bar{\varphi}_s}{\partial r} + \frac{\partial^2\bar{\eta}}{\partial r\partial z} \tag{22a}$$

$$\bar{u}_z = \frac{\partial\bar{\varphi}_f}{\partial z} + \frac{\partial\bar{\varphi}_s}{\partial z} - \frac{1}{r}\frac{\partial}{\partial r}\left(r\frac{\partial\bar{\eta}}{\partial r}\right) \tag{22b}$$

And the pore pressure has the same expression as Eq. (8b).

To derive the general solution for the porous medium in the cylindrical coordinate system (r,θ,z), the Hankel integral transform is required [14,15]. The mth-order Hankel transform is defined by [16]

$$\hat{f}^{(m)}(\xi) = \int_0^{+\infty} rf(r)J_m(\xi r)\, dr, \quad f(r) = \int_0^{+\infty} \xi\hat{f}^{(m)}(\xi)J_m(\xi r)\, d\xi \tag{23}$$

where $J_m^{(*)}$ denotes the mth-order first kind of Bessel function and ξ denotes the Hankel transform parameter.

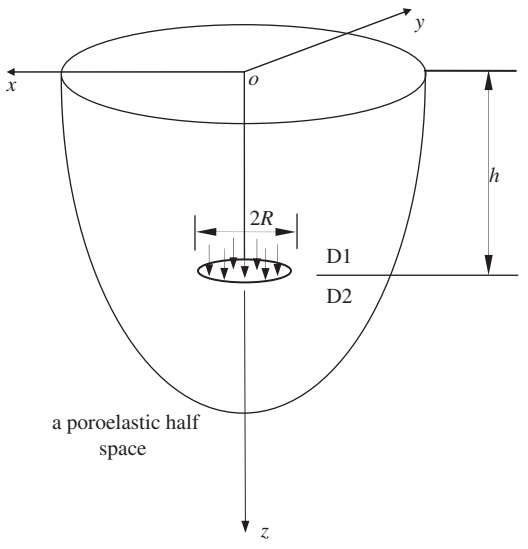

Fig. 2. Vertical uniform circular patch load applied in a poroelastic half-space.

In terms of the potentials and using the Hankel integral transform with respect to the radial coordinate r, the expressions for the displacements, stresses and the pore pressure in the frequency–wavenumber domain are expressed as follows [18]:

$$\begin{aligned}
\widetilde{\bar{u}}_z^{[0]}(\xi,z,\omega) &= \delta_f[A(\xi,\omega)\mathrm{e}^{\delta_f z} - B(\xi,\omega)\mathrm{e}^{-\delta_f z}] + \delta_s[C(\xi,\omega)\mathrm{e}^{\delta_s z} - D(\xi,\omega)\mathrm{e}^{-\delta_s z}] \\
&\quad + \xi^2[E(\xi,\omega)\mathrm{e}^{\delta_t z} + F(\xi,\omega)\mathrm{e}^{-\delta_t z}] \\
\widetilde{\bar{u}}_r^{[1]}(\xi,z,\omega) &= -\xi[A(\xi,\omega)\mathrm{e}^{\delta_f z} + B(\xi,\omega)\mathrm{e}^{-\delta_f z} + C(\xi,\omega)\mathrm{e}^{\delta_s z} + D(\xi,\omega)\mathrm{e}^{-\delta_s z}] \\
&\quad + \xi\delta_t[E(\xi,\omega)\mathrm{e}^{\delta_t z} - F(\xi,\omega)\mathrm{e}^{-\delta_t z}] \\
\widetilde{\bar{p}}_f^{[0]}(\xi,z,\omega) &= -A_f k_f^2[A(\xi,\omega)\mathrm{e}^{\delta_f z} + B(\xi,\omega)\mathrm{e}^{-\delta_f z}] - A_s k_s^2[C(\xi,\omega)\mathrm{e}^{\delta_s z} + D(\xi,\omega)\mathrm{e}^{-\delta_s z}] \\
\widetilde{\bar{\sigma}}_{zz}^{[0]}(\xi,z,\omega) &= [2\mu\delta_f^2 + \lambda(\delta_f^2 - \xi^2) - \alpha A_f k_f^2][A(\xi,\omega)\mathrm{e}^{\delta_f z} + B(\xi,\omega)\mathrm{e}^{-\delta_f z}] \\
&\quad + [2\mu\delta_s^2 + \lambda(\delta_s^2 - \xi^2) - \alpha A_s k_s^2][C(\xi,\omega)\mathrm{e}^{\delta_s z} + D(\xi,\omega)\mathrm{e}^{-\delta_s z}] \\
&\quad + 2\mu\delta_t\xi^2[E(\xi,\omega)\mathrm{e}^{\delta_t z} - F(\xi,\omega)\mathrm{e}^{-\delta_t z}] \\
\widetilde{\bar{\sigma}}_{zr}^{[1]}(\xi,z,\omega) &= -2\mu\xi\Big\{\delta_f[A(\xi,\omega)\mathrm{e}^{\delta_f z} - B(\xi,\omega)\mathrm{e}^{-\delta_f z}] + \delta_s[C(\xi,\omega)\mathrm{e}^{\delta_s z} - D(\xi,\omega)\mathrm{e}^{-\delta_s z}] \\
&\quad + \frac{k_t^2}{2}[E(\xi,\omega)\mathrm{e}^{\delta_t z} + F(\xi,\omega)\mathrm{e}^{-\delta_t z}]\Big\}
\end{aligned} \tag{24a - e}$$

where $A(\xi,\omega)$–$F(\xi,\omega)$ are the arbitrary constants, δ_f, δ_s and δ_t are complex numbers related to the vertical wavenumbers for the P_1, the P_2 and the S wave of the porous medium and

$$\delta_f = \sqrt{\xi^2 - k_f^2}, \quad \delta_s = \sqrt{\xi^2 - k_s^2}, \quad \delta_t = \sqrt{\xi^2 - k_t^2} \tag{25}$$

Note that the real part of δ_α, $\alpha = f, s, t$ in Eq. (25) should be always non-negative.

For the D1 domain (Fig. 2), the general solution in Eqs. (24a–e) have six unknown constants to be determined, while for the domain D2 (Fig. 2), due to the bounded condition at infinity, only three constants remain. For a permeable surface, the boundary conditions of the surface of D1 are as follows (Fig. 2):

$$\widetilde{\bar{\sigma}}_{zz}^{[0]}(\xi,0,\omega) = 0, \quad \widetilde{\bar{\sigma}}_{zr}^{[1]}(\xi,0,\omega) = 0, \quad \widetilde{\bar{p}}_f^{[0]}(\xi,0,\omega) = 0 \tag{26}$$

At the interface between the D1 and the D2 domain, the continuity conditions are as follows (Fig. 2):

$$\begin{aligned}
&\widetilde{\bar{u}}_r^{[1]}(\xi,h^-,\omega) = \widetilde{\bar{u}}_r^{[1]}(\xi,h^+,\omega), \quad \widetilde{\bar{u}}_z^{[0]}(\xi,h^-,\omega) = \widetilde{\bar{u}}_z^{[0]}(\xi,h^+,\omega), \\
&\widetilde{\bar{w}}_z^{[0]}(\xi,h^-,\omega) = \widetilde{\bar{w}}_z^{[0]}(\xi,h^+,\omega), \quad \widetilde{\bar{p}}_f^{[0]}(\xi,h^-,\omega) = \widetilde{\bar{p}}_f^{[0]}(\xi,h^+,\omega), \\
&\widetilde{\bar{\sigma}}_{zz}^{[0]}(\xi,h^+,\omega) - \widetilde{\bar{\sigma}}_{zz}^{[0]}(\xi,h^-,\omega) = -\frac{RJ_1(R\xi)}{A\xi}, \quad \widetilde{\bar{\sigma}}_{zr}^{[1]}(\xi,h^-,\omega) = \widetilde{\bar{\sigma}}_{zr}^{[1]}(\xi,h^+,\omega)
\end{aligned} \tag{27}$$

The nine unknown constants for the D1 and the D2 domain can be calculated by nine linear algebraic equations (26) and (27). Substitution of the obtained constants into Eq. (24) and inversion of the Hankel transform give the frequency domain fundamental solution.

3. Fredholm integral equations describing dynamic interaction between piles and the poroelastic half-space

As shown in Fig. 1, the pile rows embedded in the poroelastic half-space is used to isolate the vibration generated by a moving load. The number of the total pile is $m = \sum_{k=1}^{K} n_k$, where K, n_k denote the number of pile rows and the number of the piles in the kth row. The spacing between two neighboring piles in each pile row is denoted by s. Also, it is assumed that each pile has the same diameter d ($d = 2R$) and the same length L ($d/L \ll 1$). A vertical moving load with a constant speed c and an oscillating frequency ω_0 is acted on the surface of the poroelastic half-space and moves along the positive direction of the y-axis (Fig. 1).

When the pile-half-space system is subjected to a vertical moving load, generally, the pile will experience both vertical and horizontal response. However, as the influence of the horizontal interaction between the pile–soil system is relatively smaller, the horizontal interaction between piles and the half-space is neglected in this paper. Thus, only the vertical interaction between the piles and the half-space is considered in the paper. Moreover, the exact hydraulic boundary condition on the pile–soil interface is ignored in this study [19].

Following Muki and Sternberg [14,15] and Pak and Jennings [20], the current problem is decomposed into two sub-problems: an extended poroelastic half-space and multiple fictitious piles. The response of the poroelastic half-space is governed by Biot's theory, while the fictitious pile is described by the one-dimensional bar vibration theory. The decomposition procedure is illustrated in Fig. 3 by the ith pile of the pile rows.

For the fictitious piles, Young's modulus ($E_{p*}^{(i)}$) and the density ($\rho_{p*}^{(i)}$) of the fictitious ith pile are expressed as [14,15]

$$E_{p*}^{(i)} = E_p^{(i)} - E_s, \quad \rho_{p*}^{(i)} = \rho_p^{(i)} - \rho, \quad i = 1, 2, \ldots, m \tag{28}$$

where $E_p^{(i)}$ and E_s are Young's modulus for the ith pile and the poroelastic half-space, $E_s = \mu(3\lambda + 2\mu)/(\lambda + \mu)$, $\rho_p^{(i)}$, ρ are the densities for the ith pile and the poroelastic half-space, while $E_{p*}^{(i)}$ and $\rho_{p*}^{(i)}$ are Young's modulus and the density of the ith fictitious pile.

It is assumed that the axial force of the ith fictitious pile is $\bar{N}_*^{(i)}(z,\omega)$ and the vertical distributed load along the ith fictitious pile is $\bar{q}_z^{(i)}(z,\omega)$ (Fig. 3(b)). The top and the bottom of the ith fictitious pile are subjected to forces $\bar{N}_*^{(i)}(0,\omega)$, $\bar{N}_*^{(i)}(L,\omega)$, respectively. The poroelastic half-space are subjected to the following loads (Fig. 3(a)): $\bar{q}_z^{(i)}(z,\omega)$ that is distributed over the region occupied by the ith pile; $\bar{N}_*^{(i)}(0,\omega)/A^{(i)}$ and $\bar{N}_*^{(i)}(L,\omega)/A^{(i)}$ which are applied to the circular area $\Pi_0^{(i)}$ and $\Pi_L^{(i)}$, respectively. Note that $A^{(i)}$ denotes the cross-section area of the ith pile.

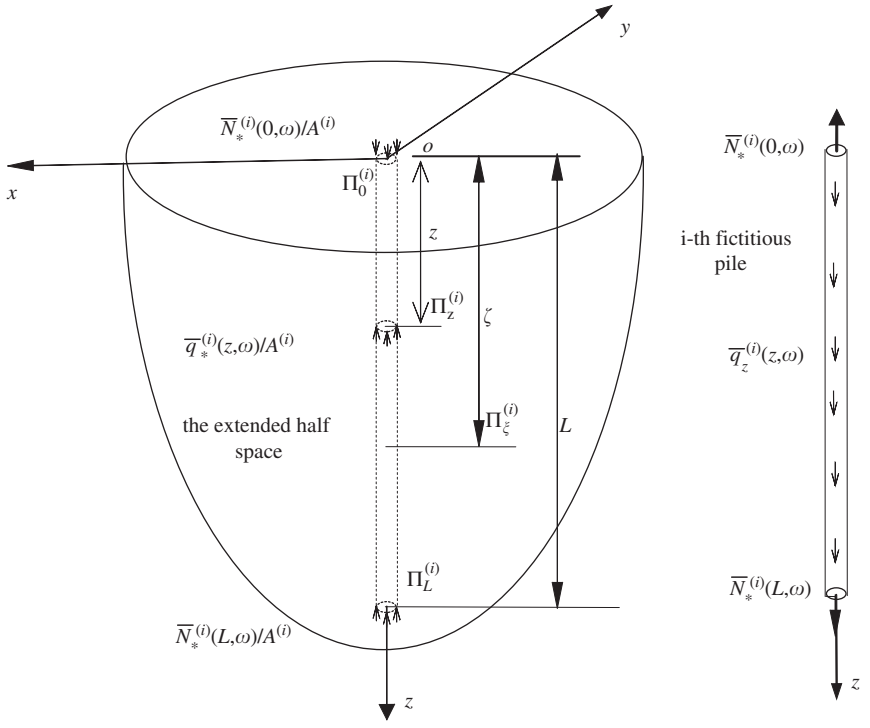

Fig. 3. The model for the decomposition of the pile-half-space system.

For the ith fictitious pile, the displacement $\bar{u}^{(i)}_{zp*}(z,\omega)$, the distributed vertical force $\bar{q}^{(i)}_z(z,\omega)$ and the axial force satisfy the following relations:

$$\bar{q}^{(i)}_z(z,\omega) = -\frac{\mathrm{d}\bar{N}^{(i)}_*(z,\omega)}{\mathrm{d}z} - \rho^{(i)}_{p*}A^{(i)}\omega^2\bar{u}^{(i)}_{zp*}(z,\omega), \quad i = 1,2,\ldots,m \tag{29a}$$

$$\bar{u}^{(i)}_{zp*}(z,\omega) = \bar{u}^{(i)}_{zp*}(0,\omega) + \frac{1}{E^{(i)}_{p*}A^{(i)}}\int_0^z \bar{N}^{(i)}_*(\eta,\omega)\,\mathrm{d}\eta, \quad i = 1,2,\ldots,m \tag{29b}$$

in which $\bar{u}^{(i)}_{zp*}(z,\omega)$ is the vertical displacement of the ith pile.

The vertical strain of the extended half-space along the axis of the ith pile is composed of two parts: the first part is due to the free wave field, while the second part is due to the force applied to the extended half-space by the fictitious piles. Thus, the vertical strain of the extended half-space along the axis of the ith pile can be written as

$$\begin{aligned}\bar{\varepsilon}^{(i)}_{zs}(z,\omega) = \bar{\varepsilon}^{(i)}_{zf}(z,\omega) + \sum_{j=1}^{m}\Bigg[&\bar{N}^{(j)}_*(0,\omega)\bar{\varepsilon}^{(G)}_z(r_{ij},0,z,\omega) - \bar{N}^{(j)}_*(L,\omega)\bar{\varepsilon}^{(G)}_z(r_{ij},L,z,\omega)\\ &- \int_0^{L_j}\bar{q}^{(j)}_z(\zeta,\omega)\bar{\varepsilon}^{(G)}_z(r_{ij},\zeta,z,\omega)d\zeta\Bigg], \quad i = 1,2,\ldots\ldots,m\end{aligned} \tag{30}$$

where the superscript and subscript i, j denote the ith and the jth pile, respectively, $\bar{\varepsilon}^{(i)}_{zf}(z,\omega)$ is the free field vertical strain at the axis of the ith pile, which is determined by the free field frequency domain solution of the moving load, and $\bar{\varepsilon}^{(G)}_z(r_{ij},\zeta,z,\omega)$ represents the vertical strain at the center of $\Pi^{(i)}_z$ due to a unit patch load applied at $\Pi^{(j)}_\zeta$ (Fig. 3(a)) and r_{ij} is the horizontal distance between the axis of the ith and jth pile. It is worth noting that for the case $i = j$, r_{ij} is vanishing.

Using Eqs. (29) and (30), the following relation is obtained:

$$\begin{aligned}\bar{\varepsilon}^{(i)}_{zs}(z,\omega) = \bar{\varepsilon}^{(i)}_{zf}(z,\omega) &- \bar{N}^{(i)}_*(z,\omega)[\bar{\varepsilon}^{(G)}_z(r_{ii},z^+,z,\omega) - \bar{\varepsilon}^{(G)}_z(r_{ii},z^-,z,\omega)]\\ &- \int_0^{L_i}\bar{N}^{(i)}_*(z,\omega)\frac{\partial\bar{\varepsilon}^{(G)}_z(r_{ii},\zeta,z,\omega)}{\partial\zeta}\,\mathrm{d}\zeta + \rho^{(i)}_{p*}A^{(i)}\omega^2\int_0^{L_i}\bar{u}^{(i)}_{zp*}(\zeta,\omega)\bar{\varepsilon}^{(G)}_z(r_{ii},\zeta,z,\omega)\,\mathrm{d}\zeta\\ &+ \sum_{j=1}^{m(j\neq i)}\left[-\int_0^{L_i}\bar{N}^{(j)}_*(\zeta,\omega)\frac{\partial\bar{\varepsilon}^{(G)}_z(r_{ij},\zeta,z,\omega)}{\partial\zeta}\,\mathrm{d}\zeta + \rho^{(j)}_{p*}A^{(j)}\omega^2\int_0^{L_i}\bar{u}^{(j)}_{zp*}(\zeta,\omega)\bar{\varepsilon}^{(G)}_z(r_{ij},\zeta,z,\omega)\,\mathrm{d}\zeta\right]\\ &i = 1,2,\ldots,m\end{aligned} \tag{31}$$

where $\bar{\varepsilon}^{(G)}_z(r_{ii},z^-,z,\omega)$, $\bar{\varepsilon}^{(G)}_z(r_{ii},z^+,z,\omega)$ denote the vertical strain of the poroelastic half-space at the center of $\Pi^{(i)}_z$ of the ith pile when the patch load $\Pi^{(i)}_\xi$ approaches $\Pi^{(i)}_z$ from up and down side, respectively.

In this study, the compatibility condition between the ith pile and the poroelastic half-space is fulfilled by requiring the vertical strain of the ith fictitious pile and that of the extended half-space along the axis of the ith fictitious pile to be equal

$$\bar{\varepsilon}^{(i)}_{zp*}(z,\omega) = \bar{\varepsilon}^{(i)}_{zs}(z,\omega), \quad 0\leqslant z\leqslant L, \quad i = 1,2,\ldots,m \tag{32}$$

where $\bar{\varepsilon}^{(i)}_{zp*}(z,\omega)$ represents the vertical strain of the ith fictitious pile.

Using Eqs. (29), (31) and (32), the Fredholm integral equation in the frequency domain describing the vertical interaction between the ith pile and the half-space has the form

$$\begin{aligned}\frac{\bar{N}^{(i)}_*(z,\omega)}{E^{(i)}_{p*}A^{(i)}} + \bar{N}^{(i)}_*(z,\omega)\left[\bar{\varepsilon}^{(G)}_z(r_{ii},z^+,z,\omega) - \bar{\varepsilon}^{(G)}_z(r_{ii},z^-,z,\omega)\right] + \sum_{j=1}^{m}\Bigg[&\int_0^{L_j}\bar{N}^{(j)}_*(\zeta,\omega)\frac{\partial\bar{\varepsilon}^{(G)}_z(r_{ij},\zeta,z,\omega)}{\partial\zeta}\,\mathrm{d}\zeta\\ &- \int_0^{L_j}\bar{N}^{(j)}_*(\zeta,\omega)\bar{\chi}^{(a)}_{ij}(\zeta,z,\omega)\,\mathrm{d}\zeta - \bar{u}^{(j)}_{zp*}(0,\omega)\bar{\chi}^{(b)}_{ij}(z,\omega)\Bigg] = \bar{\varepsilon}^{(i)}_{zf}(z,\omega), \quad i = 1,2,\ldots,m\end{aligned} \tag{33}$$

where

$$\bar{\chi}_{ij}^{(a)}(\zeta,z,\omega)=\left(\rho_{p*}^{(j)}\omega^2/E_{p*}^{(j)}\right)\int_{\zeta}^{L_j}\bar{\varepsilon}_z^{(G)}(r_{ij},\eta,z,\omega)\,\mathrm{d}\eta,\quad \bar{\chi}_{ij}^{(b)}(z,\omega)=\rho_{p*}^{(j)}A^{(j)}\omega^2\int_{\zeta}^{L_j}\bar{\varepsilon}_z^{(G)}(r_{ij},\eta,z,\omega)\,\mathrm{d}\eta \tag{34}$$

Following the similar procedures, the surface vertical displacement $\bar{u}_{zs}(\mathbf{x}_\perp,z=0,\omega)$ for the poroelastic half-space in the presence of the pile rows can be calculated as follows:

$$\bar{u}_{zs}(\mathbf{x}_\perp,0,\omega)=\bar{u}_{zf}(\mathbf{x}_\perp,0,\omega)+\sum_{j=1}^{m}\left[-\int_0^{L_j}\bar{N}_*^{(j)}(\zeta,\omega)\frac{\partial\bar{u}^{(G)}(r_{\mathbf{x}_\perp j},\zeta,0,\omega)}{\partial\zeta}\,\mathrm{d}\zeta\right.$$
$$\left.+\rho_{p*}^{(j)}A^{(j)}\omega^2\int_0^{L_j}\bar{u}_{zp*}^{(j)}(\zeta,\omega)\bar{u}^{(G)}(r_{\mathbf{x}_\perp j},\zeta,0,\omega)\,\mathrm{d}\zeta\right] \tag{35}$$

where $\bar{u}_{zf}^{(S)}(\mathbf{x}_\perp,0,\omega)$ represents the free field vertical displacement, $\bar{u}^{(G)}(r_{\mathbf{x}_\perp j},\zeta,0,\omega)$ denotes the vertical displacement at the surface point $\mathbf{x}_\perp$ ($\mathbf{x}_\perp=x\mathbf{i}+y\mathbf{j}$) due to a unit patch load applied at $\Pi_\xi^{(j)}$, $r_{\mathbf{x}_\perp j}$ is the horizontal distance between the surface point $\mathbf{x}_\perp$ and the axis of the jth pile.

In Eq. (33), the vertical displacement of the ith pile top $\bar{u}_{zp*}^{(i)}(0,\omega)$ is also unknown. The unknown $\bar{u}_{zp*}^{(i)}(0,\omega)$ can be represented by the axial force of the fictitious piles if the vertical displacement of the ith pile top and the surface vertical displacement of the extended half-space at the center of the ith pile top are assumed to be equal, i.e., $\bar{u}_{zp*}^{(i)}(0,\omega)=\bar{u}_{zs}^{(i)}(0,\omega)$. Note that $\bar{u}_{zs}^{(i)}(0,\omega)$ can be obtained via Eq. (35) by setting $\mathbf{x}_\perp$ coincide with the center of the ith pile. Thus, using Eqs. (29) and (35), the following supplementary equations for $\bar{u}_{zp*}^{(i)}(0,\omega)$ are derived:

$$\sum_{j=1}^{m}\left[-\int_0^{L_j}\bar{N}_*^{(j)}(\zeta,\omega)\frac{\partial\bar{u}^{(G)}(r_{ij},\zeta,0,\omega)}{\partial\zeta}\right]\mathrm{d}\zeta+\sum_{j=1}^{m}\int_0^{L_j}\bar{N}_*^{(j)}(\zeta,\omega)\bar{\chi}_{ij}^{(c)}(\zeta,0,\omega)\,\mathrm{d}\zeta$$
$$+\sum_{j=1}^{m}\bar{u}_{zp*}^{(j)}(0,\omega)\left[\bar{\chi}_{ij}^{(d)}(0,\omega)-\delta_{ij}\right]=-\bar{u}_{zf}^{(i)}(0,\omega),\quad i=1,2,\ldots,m \tag{36}$$

where δ_{ij} is the Kronecker delta and

$$\bar{\chi}_{ij}^{(c)}(\zeta,z,\omega)=\frac{\rho_{pj*}^{(j)}\omega^2}{E_{pj*}^{(j)}}\int_{\zeta}^{L_j}\bar{u}^{(G)}(r_{ij},\eta,z,\omega)\,\mathrm{d}\eta,\quad \bar{\chi}_{ij}^{(d)}(z,\omega)=\rho_{p*}^{(j)}A^{(j)}\omega^2\int_0^{L_j}\bar{u}^{(G)}(r_{ij},\eta,z,\omega)\,\mathrm{d}\eta \tag{37}$$

4. Definition of the amplitude reduction ratio

To assess the vibration isolation effect of pile rows, the amplitude reduction ratio A_r at point $\mathbf{x}_\perp$, which is the ratio between the amplitude of the surface vertical displacement of the half-space in the presence of the pile rows and that of the free field solution, is defined as follows:

$$A_r(\mathbf{x}_\perp,t)=\frac{\left|u_{zs}(\mathbf{x}_\perp,z=0,t)\right|}{\left|u_{zf}(\mathbf{x}_\perp,z=0,t)\right|} \tag{38}$$

where $\left|u_{zs}(\mathbf{x}_\perp,z=0,t)\right|$ is the amplitude of the vertical displacement of the half-space in the presence of the pile rows, $\left|u_{zf}(\mathbf{x}_\perp,z=0,t)\right|$ is the amplitude of the vertical displacement of the soil given by the free field solution.

Woods [21] proposed an average amplitude reduction ratio $\bar{A}_r$ for the evaluation of vibration isolation effect, which is defined as follows:

$$\bar{A}_r=\frac{1}{A}\int_A A_r\,\mathrm{d}A \tag{39}$$

where A is the area of a rectangle with its width and length determined by the Rayleigh wavelength and the width of pile rows.

5. Numerical results and discussions

The integral equations in the frequency domain accounting for the vertical interaction between pile rows and the half-space can be solved numerically. The methodology for solving integral equation (33) was detailed in Ref. [20]. After discretization of Eqs. (33) and (36), the following linear algebraic equations in the frequency domain are obtained:

$$\mathbf{A}(\omega)\mathbf{X}(\omega) = \mathbf{b}(\omega) \tag{40}$$

where $\mathbf{A}(\omega)$ is the coefficient matrix determined by discrete integral equations which is associated with the fundamental solution, $\mathbf{b}(\omega)$ is the right-handed term which is determined by the free field solution, such as, $\bar{\varepsilon}_z^{(f)}(x,y,z,\omega)$, and $\mathbf{X}(\omega)$ is the discrete unknowns of the integral equations.

In order to recover the time domain solution, a series of frequency domain solutions at discrete sample points have to be determined first. Assuming the number of the frequency domain sample points is $2N+1$, then, Eq. (40) for the sample points $i = 1, 2, \ldots, N, N+1$ has the following form:

$$\mathbf{A}(\omega)\big|_{\omega=(i-1)\Delta\omega}\mathbf{X}(\omega)\big|_{\omega=(i-1)\Delta\omega} = \mathbf{b}(\omega)\big|_{\omega=(i-1)\Delta\omega}, \quad i = 1, 2, \ldots, N, N+1 \tag{41}$$

where $\Delta\omega$ is the frequency increment for the sample points in the frequency domain and given by

$$\Delta\omega = \frac{2\pi}{T}, \quad T = \frac{2y_0}{c} \tag{42}$$

In order to account for the maximum frequency component involved in the response of the pile–soil system due to the moving load, the time increment has to fulfill the following relation [22]:

$$\Delta t = \frac{T}{2N+1} \leqslant \frac{\pi}{\omega_{\max}} \tag{43}$$

where $\omega_{\max}$ is the maximum frequency in the response of the pile–soil system, which can be determined by the analysis of the free field solution in the frequency domain. Also, the coordinate y_0 of the moving load at the time $t = 0$ should be large enough to make the period T be able to accommodate the main response of the concerned domain (e.g., pile rows and the neighboring domain). Note that to avoid the Nyquist component, the sample points in the frequency domain should be an odd number [23], which is set to be $2N+1$ in this study.

According to the property of the discrete Fourier transform [22], $\mathbf{A}(\omega)$ in Eq. (40) for the sample points $i = N+2, \ldots, 2N+1$ is given by the following relation:

$$[\mathbf{A}(\omega)]_i = \mathrm{Conjg}\{\mathbf{A}(\omega)\big|_{\omega=[(2N+2)-i]\Delta\omega}\}, \quad i = N+2, \ldots, 2N+1 \tag{44}$$

Due to the vibration frequency ω_0 of the moving load in Eqs. (13) and (15), the right-handed term $\mathbf{b}(\omega)$ for the sample points $i = N+2, \ldots, 2N+1$ should be determined by the following equation:

$$[\mathbf{b}(\omega)]_i = \mathbf{b}(\omega)\big|_{\omega=-[(2N+2)-i]\Delta\omega}, \quad i = N+2, \ldots, 2N+1 \tag{45}$$

After numerical solution of the integral equation (33) for the sample points $i = 1, 2, \ldots, N+1, \quad N+2, \ldots, 2N+1$, all the variables in the frequency domain are obtained. The time domain solution for the variables can be obtained by performing inverse Fourier transform on the corresponding frequency domain solutions, which is implemented by the FFT method in this study [22].

In the numerical examples, we use a single pile row of 10 piles with the circular cross-section as a passive isolation vibration facility. The load moves along a line parallel to the y-axis in the positive y direction. Each pile has the same diameter d, the same length L, the same Young's modulus E_p and the same density ρ_p. The material parameters for the poroelastic half-space are given as follows: $\mu = 1.32 \times 10^8$ N/m^2, $\lambda = 1.32 \times 10^8$ N/m^2, $M = 1.0 \times 10^{11}$ N/m^2, $\rho_s = 2.0 \times 10^3$ kg/m^3, $\rho_f = 1.0 \times 10^3$ kg/m^3, $\phi = 0.4$, $\alpha = 0.97$, $b_p = 1.9 \times 10^7$ kg/m^{3}s, $a_\infty = 3.0$.

In calculation, when evaluating Eq. (39), the Rayleigh wave wavelength needs to be determined in advance. In this study, the Rayleigh wave wavelength in Eq. (39) is assumed to be the Rayleigh wave of an elastic medium, and the frequency of the Rayleigh wave is equal to the oscillating frequency of the moving load (ω_0). Also, the elastic medium assumes the same material parameters as the solid skeleton of the porous medium.

For example, when $f = 50\,\text{Hz}$, $\mu = 1.32 \times 10^8\ \text{N/m}^2$, $\lambda = 1.32 \times 10^8\ \text{N/m}^2$, $\rho = 2.0 \times 10^3\ \text{kg/m}^3$, the Rayleigh wave wavelength takes $\lambda_R = 5.0\,\text{m}$.

To verify our method, in Section 5.1, a special case of the present paper is compared with some known results. In Sections 5.2–5.5, some numerical examples and corresponding analysis are presented.

5.1. Comparison of our results with known results

In this section, the method developed in this study is justified by comparing results of this research with existing results. As shown in Fig. 1, the vibration source is a vertical moving distributed load moving parallelly to the y-axis at a constant speed c. The magnitude of the load is 100 kN and its vibration frequency is $f = 50\,\text{Hz}$. The moving load is uniformly distributed over a rectangle with $2a \times 2b = 0.8\,\text{m}$. A single pile row with 10 piles with circular cross-section is used as the passive isolation vibration system. Each pile has the same diameter $d = 1.0\,\text{m}$, the same length $L = 5.0\,\text{m}$, the same Young's modulus $E_p = 3.3 \times 10^{10}\ \text{N/m}^2$ and the same density $\rho_p = 2.4 \times 10^3\ \text{kg/m}^3$. The net spacing between two neighboring piles is $s = 0.5\,\text{m}$. The distance between the y-axis and the trace of the load is $d_s = 7.5\,\text{m}$.

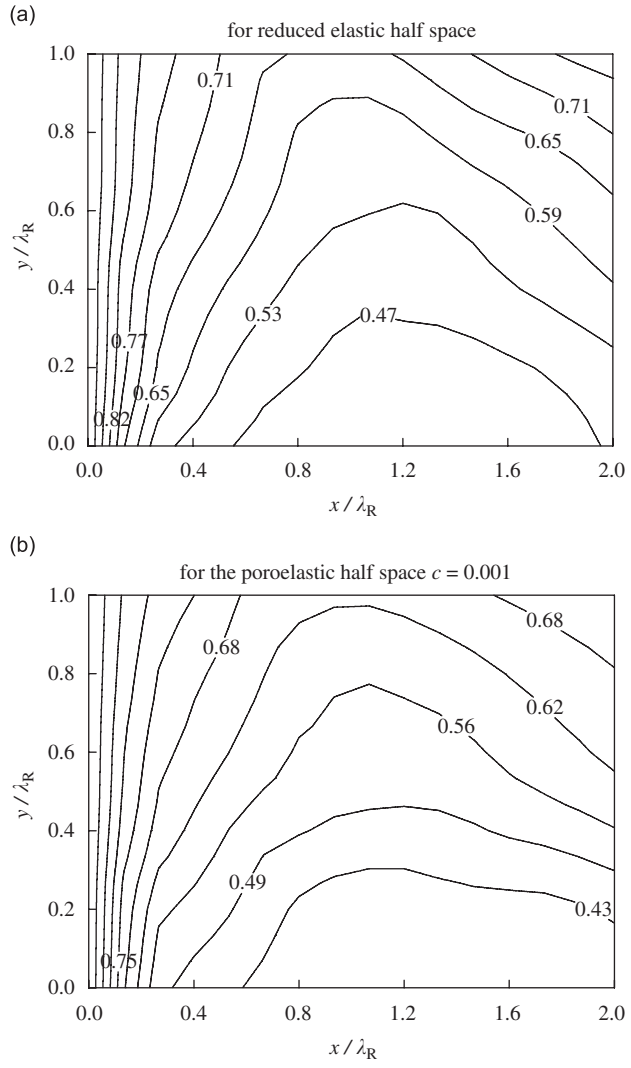

Fig. 4. The contour of the amplitude reduction ratio A_r for a single pile row with ten circular cross-section piles as passive vibration isolation system embedded in (a) the single-phase elastic medium and (b) the poroelastic medium.

Kattis et al. [5] gave the vibration isolation effect of pile rows embedded in an elastic half-space against a harmonic vertical force. To compare results of current study with Kattis', the parameters M, a_∞, α, b_p, ϕ, ρ_f for the poroelastic half-space are assumed to tend to zero, then, the poroelastic half-space is reduced to a quasi-elastic half-space.

It should be noted that for an elastic medium there are singularities in the path of the integration when calculating the fundamental solution, which makes the numerical evaluation of the integral a formidable task. However, some researchers tend to evaluate integrals of this sort using a viscoelastic model. In the viscoelastic model, the material damping is taken into account using complex Lame constants i.e., $\mu = \mu_0(1+\mathrm{i}\beta_s)$ and $\lambda = \lambda_0(1+\mathrm{i}\beta_s)$, where β_s denotes the damping ratio. In this paper, we use a damping ratio of $\beta_s = 0.05$ for the soil and $\mu_0 = 1.32 \times 10^8\ \mathrm{N/m^2}$, $\lambda_0 = 1.32 \times 10^8\ \mathrm{N/m^2}$, $\rho_s = 2.0 \times 10^3\ \mathrm{kg/m^3}$.

Moreover, if the velocity of the vertical moving distributed load approaches zero, the moving vibration load is reduced to a fixed time-harmonic force. In calculation, the wavelength for the Rayleigh wave of the reduced elastic medium is $\lambda_R = 5.0\,\mathrm{m}$.

According to the proposed method, the average amplitude reduction ratio $\bar{A}_r$ of the ten-pile row embedded in the quasi-elastic medium is 0.6212 when the moving load with velocity $c = 0.001\,\mathrm{m/s}$ is located at the point $(x, y, z) = (-7.5, 0, 0\,\mathrm{m})$, while the result of Kattis et al. [5] is 0.624, the difference of which is 0.45%.

Moreover, according to our method, the amplitude reduction ratio A_r for the case of the moving load located at the point $(x, y, z) = (-7.5, 0, 0\,\mathrm{m})$ for the reduced elastic medium and the poroelastic medium are also shown in Fig. 4(a) and (b), respectively. The average amplitude reduction ratio for the poroelastic half-space is $\bar{A}_r = 0.595$. Thus, we can see that that for the same pile row and the same vibration source, the vibration isolation effect of the poroelastic medium is better than that for the single-phase elastic medium.

Fig. 5 shows that the amplitude reduction ratio A_r along $0 \leqslant x/\lambda_R \leqslant 2$ when the moving load located at the point $(x, y, z) = (-7.5, 0, 0\,\mathrm{m})$ for the elastic and the poroelastic half-space. Note that $x = 0$ represents the y-axis which passing through the centers of the piles' top (Fig. 1). It can be observed that the amplitude reduction ratio A_r right behind the pile row is larger than that at other areas for both media. For the case of the pile row in the poroelastic half-space, the minimum amplitude reduction ratio $A_r = 0.3644$ occurs at the distance of $x/\lambda_R = 1.05$, while for the elastic half-space, the minimum amplitude reduction ratio $A_r = 0.4141$ occurs at the distance of $x/\lambda_R = 0.85$.

5.2. Effects of the velocity of the moving load

In this section, the influences of the velocity of the moving load (c) on the vibration isolation effect will be examined. The vibration source is a point load with the magnitude of $F_z = 100\,\mathrm{kN}$. The point load moves

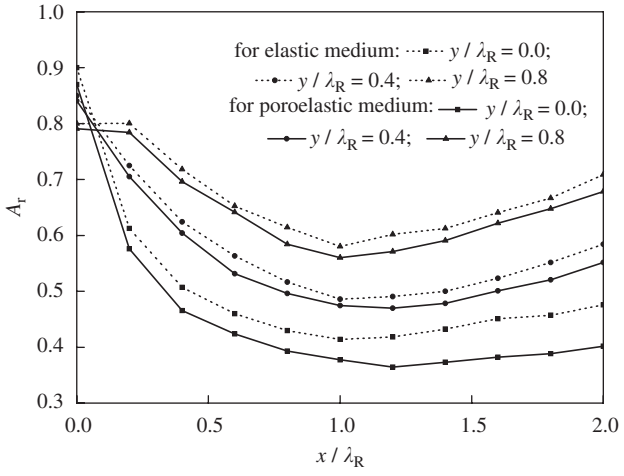

Fig. 5. The amplitude reduction ratio A_r within the range $x/\lambda_R = 0$–2 with $y/\lambda_R = 0.0$, $y/\lambda_R = \pm 0.4$ and $y/\lambda_R = \pm 0.8$, respectively, for a single pile row with ten circular cross-section piles embedded in the elastic half-space and the poroelastic half-space.

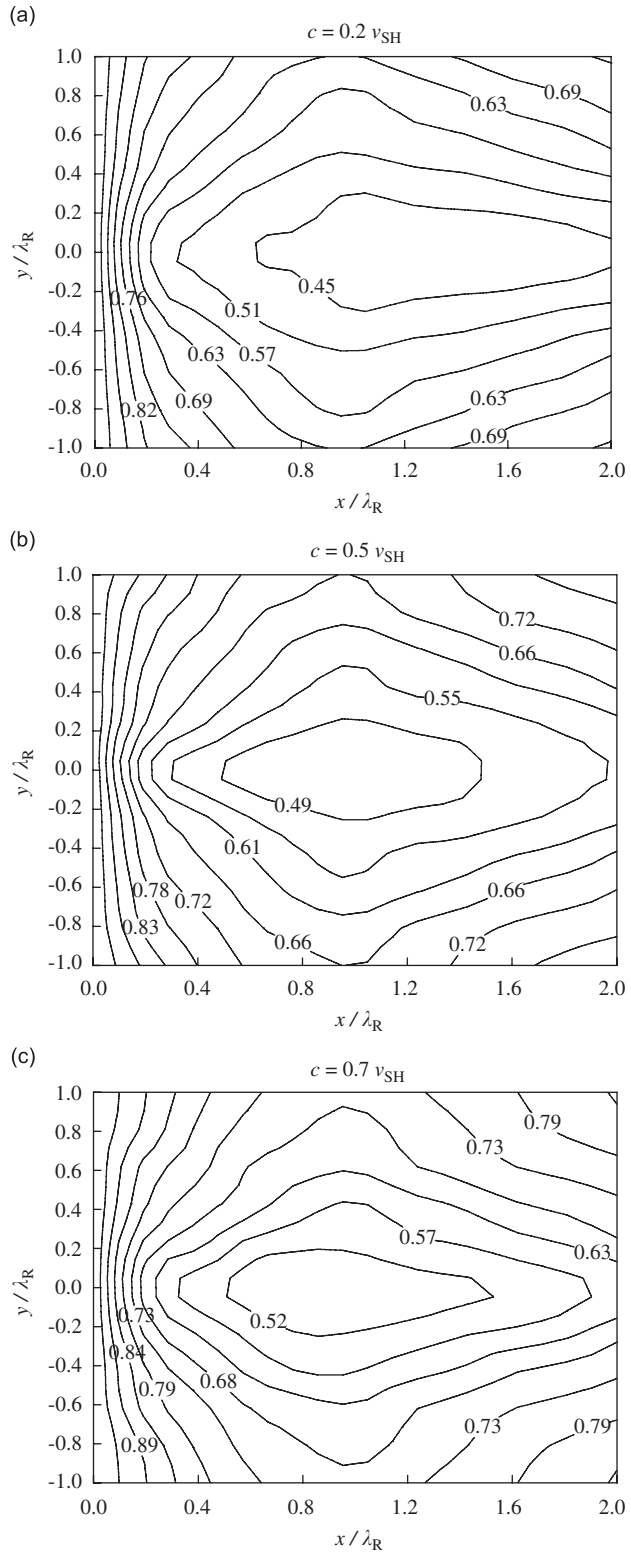

Fig. 6. The variation of the amplitude reduction ratio A_r on the surface for the poroelastic half-space at the instant when the moving load passing the point $(x, y, z) = (-7.5, 0, 0\,\mathrm{m})$ with three different velocities: (a) $c = 0.2v_{SH}$; (b) $c = 0.5v_{SH}$; (c) $c = 0.7v_{SH}$.

along a line parallel to the y-axis at a constant speed c and its vibration frequency is $f = 50$ Hz. As previously, a single pile row with ten piles is used as the passive vibration isolation system. Thus, the number of pile rows is $K = 1$ and the number of piles in the pile row is $n_1 = 10$. Each pile has a circular cross-section and has the same diameter $d = 1.0$ m, the same length $L = 5.0$ m, the same Young's modulus $E_p = 3.3 \times 10^{10}$ N/m^2 and the same density $\rho_p = 2.4 \times 10^3$ kg/m^3. The net spacing between two neighboring piles is $s = 0.5$ m. The distance between the y-axis and the trace of the load is $d_s = 7.5$ m. Three different moving load velocities $c = 0.2v_{SH}$, $c = 0.5v_{SH}$ and $c = 0.7v_{SH}$ are considered, where $v_{SH} = \sqrt{\mu/\rho}$.

Fig. 6(a)–(c) illustrates the variation of the amplitude reduction ratio A_r on the surface at the instant when the moving load with speed $c = 0.2v_{SH}$, $0.5v_{SH}$ and $0.7v_{SH}$, respectively, is located at the point $(x, y, z) = (-7.5, 0, 0\,\text{m})$. The variation of the amplitude reduction ratio A_r along $0 \leqslant x/\lambda_R \leqslant 2$, $y = 0$ for the moving load located at the point $(x, y, z) = (-7.5, 0, 0\,\text{m})$ with different velocities $c = 0.2v_{SH}$, $c = 0.5v_{SH}$ and $c = 0.7v_{SH}$ is also shown in Fig. 7.

From Figs. 6 and 7, one can see that moving load speed has some influence on the minimum amplitude reduction ratio A_r. For the case of $c = 0.001$ m/s, $\bar{A}_r = 0.595$ and the minimum amplitude reduction ratio $A_r = 0.3644$ occur at $x/\lambda_R = 1.05$; for the case of $c = 0.2v_{SH}$, $\bar{A}_r = 0.6119$ and the minimum amplitude reduction ratio $A_r = 0.3876$ occurs at $x/R_L = 0.95$; for the case of $c = 0.5v_{SH}$, $\bar{A}_r = 0.6624$ and the minimum amplitude reduction ratio $A_r = 0.4352$ occurs at $x/\lambda_R = 1.01$; for the case of $c = 0.7v_{SH}$, $\bar{A}_r = 0.6985$ and the minimum amplitude reduction ratio $A_r = 0.4628$ occurs at $x/\lambda_R = 0.9$. Also, it follows from the above numerical results that the average amplitude reduction ratio $\bar{A}_r$ increases considerably with increasing moving load velocity.

Moreover, one can see from Figs. 8(a) to (c) that the amplitude reduction ratio at the instant when the moving load is located at the point $(x, y, z) = (-7.5, 0, 0\,\text{m})$ becomes a little asymmetrical with respect to the x-axis with increasing speed: for the case of $c = 0.7v_{SH}$, the vibration isolation effect at points $y/R_L = 0.2, 0.4$ is less pronounced than that at points $y/R_L = -0.2, -0.4$, respectively. However, this phenomena does not occur for the cases of $c = 0.2v_{SH}$ and $c = 0.5v_{SH}$.

5.3. Effects of Young's modulus (E_p) of the pile

Young's modulus (E_p) of the pile is an important parameter for the design of the pile-row vibration isolation system. Herein, the influence of Young's modulus of piles on the vibration isolation effect is investigated for different moving load speeds. In this example, the vibration source and the pile row are the same as those in Section 5.2. Thus, the parameters for the moving point load and the pile row assume the same values as those

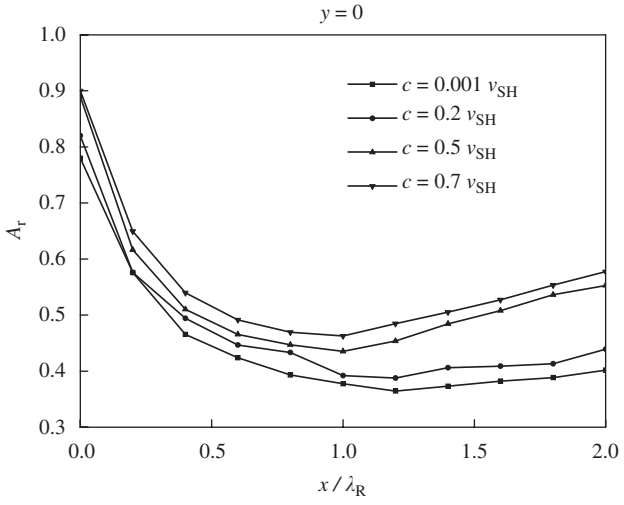

Fig. 7. The amplitude reduction ratio A_r within the range $x/\lambda_R = 0$–2 with $y/\lambda_R = 0.0$ for the instant when the moving load passing the point $(x, y, z) = (-7.5, 0, 0\,\text{m})$ with different velocities $c = 0.001v_{SH}$, $c = 0.2v_{SH}$, $0.5v_{SH}$ and $0.7v_{SH}$, respectively.

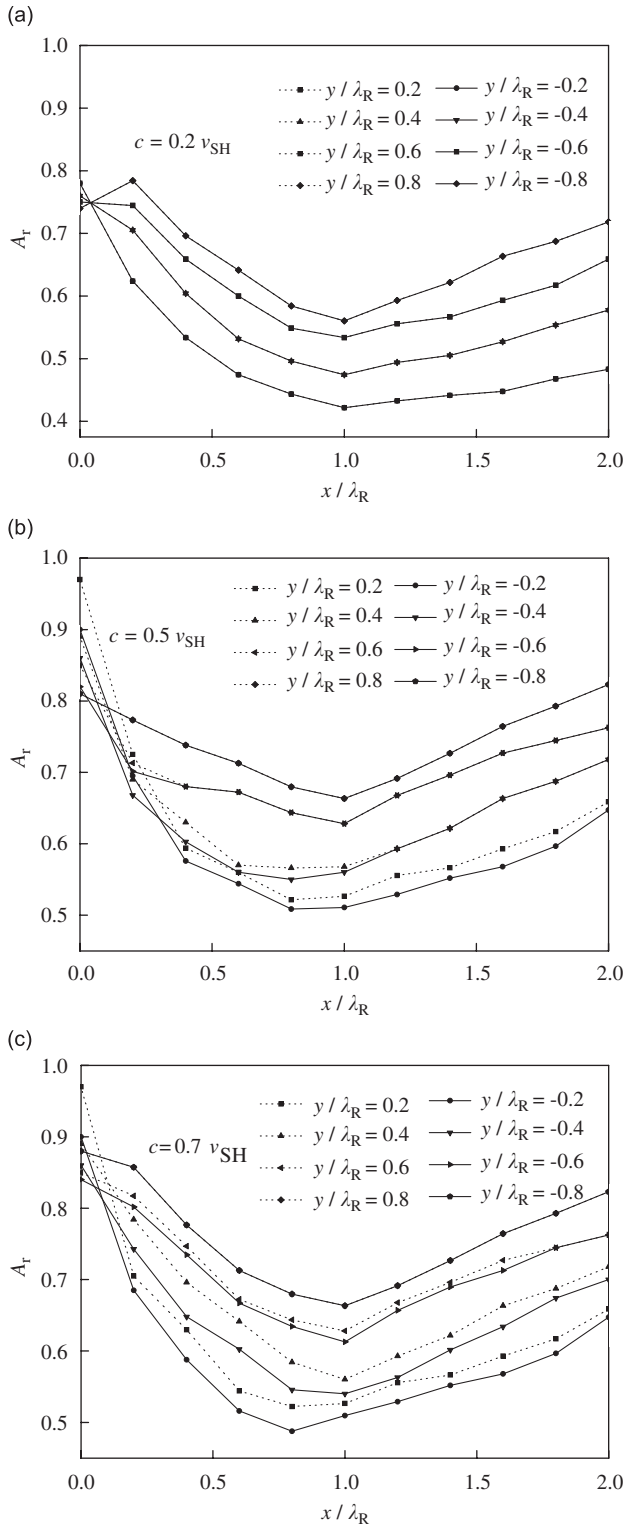

Fig. 8. The amplitude reduction ratio A_r within the range $0 \leqslant x/\lambda_R \leqslant 2$ and $y/\lambda_R = \pm 0.2$, $y/\lambda_R = \pm 0.4$, $y/\lambda_R = \pm 0.6$ and $y/\lambda_R = \pm 0.8$, respectively, for the instant of the moving load passing the point $(x, y, z) = (-7.5, 0, 0\,\mathrm{m})$ with three different velocities: (a) $c = 0.2 v_{SH}$; (b) $c = 0.5 v_{SH}$; (c) $c = 0.7 v_{SH}$.

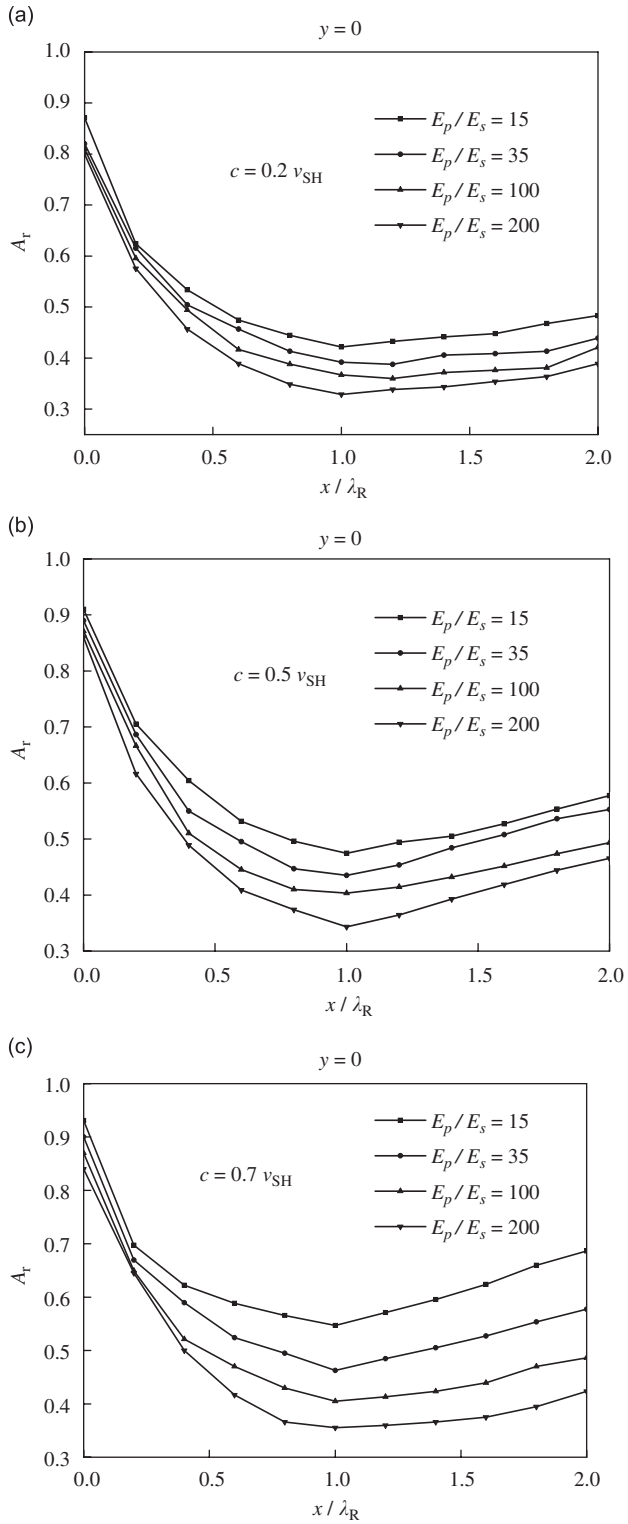

Fig. 9. The amplitude reduction ratio A_r within the range $0 \leqslant x/\lambda_R \leqslant 2$ and $y = 0$ when $E_p/E_s = 15$, 100 and 200, respectively, for the instant when the moving load passing the point $(x, y, z) = (-7.5, 0, 0\,\mathrm{m})$ with three velocities: (a) $c = 0.2v_{SH}$; (b) $c = 0.5v_{SH}$; (c) $c = 0.7v_{SH}$.

in Section 5.2 except that Young's modulus of the piles takes four different values: $E_p/E_s = 15$, 35, 100 and 200, respectively, where $E_s = \mu(3\lambda + 2\mu)/(\lambda + \mu)$. For each Young's modulus, three different values of speeds $c = 0.2v_{SH}$, $0.5v_{SH}$ and $0.7v_{SH}$ are considered with $v_{SH} = \sqrt{\mu/\rho}$.

Fig. 9(a)–(c) shows the variation of the amplitude reduction ratio A_r on the surface of the poroelastic half-space for the three cases of $E_p/E_s = 15$, 35, 100 and 200 when the moving load located at the point $(x, y, z) = (-7.5, 0, 0\,\text{m})$ with speed $c = 0.2v_{SH}$, $0.5v_{SH}$ and $0.7v_{SH}$, respectively. One can see that the minimum amplitude reduction ratio A_r occurs at almost the same location despite the variation of Young's modulus (E_p) of the pile for all the moving load speeds.

Fig. 10 shows the influence of Young's modulus ratio of E_p/E_s on the average amplitude reduction ratio $\bar{A}_r$ when the moving load located at the point $(x, y, z) = (-7.5, 0, 0\,\text{m})$ for the cases of the speed $c = 0.2v_{SH}$, $0.5v_{SH}$ and $0.7v_{SH}$, respectively. One can see that the average amplitude reduction ratio $\bar{A}_r$ decreases with increasing E_p/E_s for all the speeds, which suggests that stiffer pile row has a better vibration isolation effect. Moreover, one can see that the influence of Young's modulus (E_p) of the pile on the vibration isolation effect depends on the velocity of the moving load. When E_p/E_s increases from $E_p/E_s = 15$–200, the average amplitude reduction ratio $\bar{A}_r$ for the cases of $c = 0.2v_{SH}$, $0.5v_{SH}$ and $0.7v_{SH}$ decrease by 12.7216%, 16.8052%, 22.0283%, respectively, which indicates that for high-speed moving loads, stiffer piles are preferable for vibration isolation purpose.

5.4. Effect of the length of the piles

The influence of the length of the piles on the vibration isolation effect for different moving load speed is examined in this section. As previously, in this example, the same ten-pile row embedded in the poroelastic half-space is used to isolate the vibration due to the harmonic moving load. Also, the parameters for the moving point load and the pile row take the same values as those in Section 6.2 except that the pile length takes the following values: $L = 5.0$, 10.0, 20.0 and 50.0 m, respectively. For each pile length, three different values of moving load speeds $c = 0.2v_{SH}$, $0.5v_{SH}$ and $0.7v_{SH}$, respectively, will be calculated, where $v_{SH} = \sqrt{\mu/\rho}$.

Fig. 11(a)–(c) shows the variation of the amplitude reduction ratio A_r along $0 \leqslant x/\lambda_R \leqslant 2$, $y = 0$ for different values of $L = 10.0$, 20.0 and 50.0 m when the moving load located at the point $(x, y, z) = (-7.5, 0, 0\,\text{m})$ for the three cases of speed $c = 0.2v_{SH}$, $0.5v_{SH}$ and $= 0.7v_{SH}$, respectively. Fig. 12 plots the influence of the pile length on the average amplitude reduction ratio $\bar{A}_r$ at the instant when the moving load is at the point $(x, y, z) = (-7.5, 0, 0\,\text{m})$ for the load speed $c = 0.2v_{SH}$, $0.5v_{SH}$ and $0.7v_{SH}$, respectively.

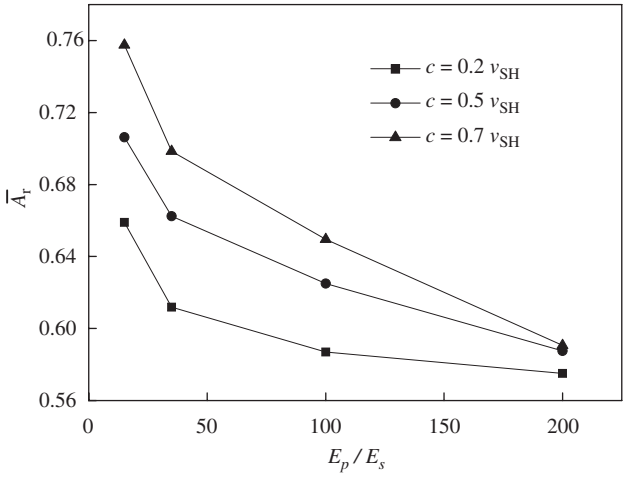

Fig. 10. The influence of Young's modulus (E_p) of the pile on the average amplitude reduction ratio $\bar{A}_r$ for the time of the moving load passing the point $(x, y, z) = (-7.5, 0, 0\,\text{m})$ with three velocities $c = 0.2v_{SH}$, $0.5v_{SH}$ and $= 0.7v_{SH}$.

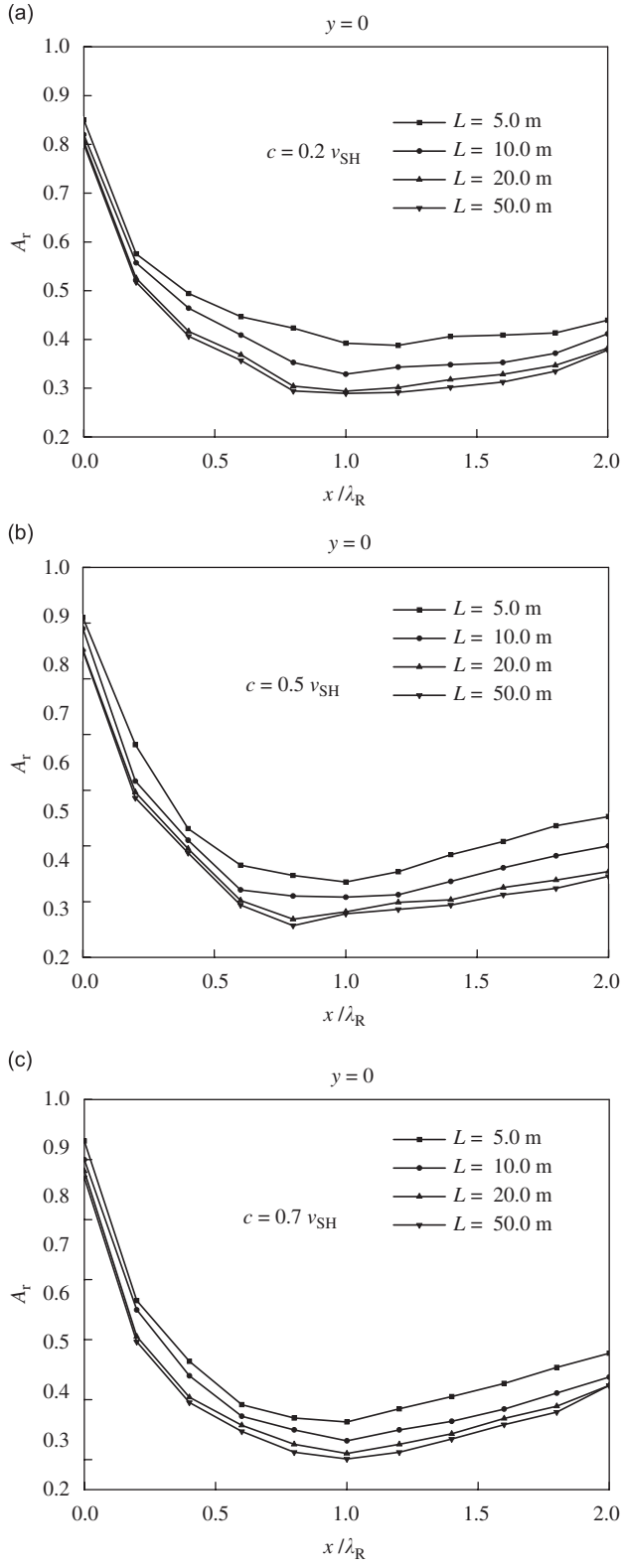

Fig. 11. The amplitude reduction ratio A_r within the range $0 \leqslant x/R_L \leqslant 2$ and $y = 0$ when $L = 5.0$, 10.0, 20.0 and 50.0 m for the time when the moving load passing the point $(x, y, z) = (-7.5, 0, 0\,\text{m})$ with three velocities: (a) $c = 0.2v_{SH}$; (b) $c = 0.5v_{SH}$; (c) $c = 0.7v_{SH}$.

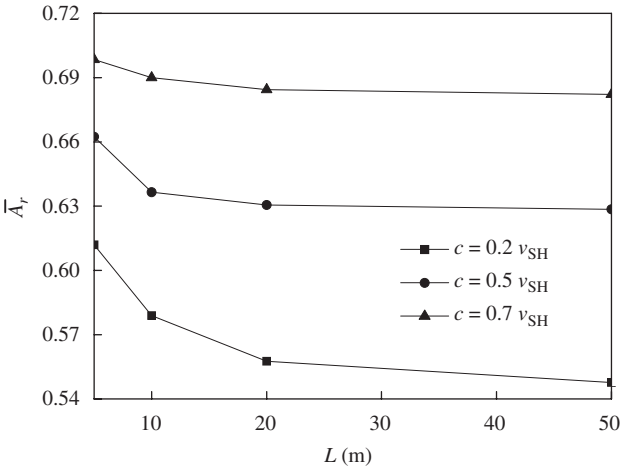

Fig. 12. The influence of pile length on the average amplitude reduction ratio $\bar{A}_r$ for the time when the moving load passing the point $(x, y, z) = (-7.5, 0, 0\,\text{m})$ with three velocities $c = 0.2v_{SH}$, $0.5v_{SH}$ and $0.7v_{SH}$, respectively.

It can be seen from Fig. 12 that the length of piles affects the average amplitude reduction ratio $\bar{A}_r$ to some extent. However, $\bar{A}_r$ only increases slightly when L/λ_R is larger than a certain value. For example, when the moving load velocity $c = 0.2v_{SH}$, the influence of pile length on the vibration isolation effect is very little when L/λ_R is greater than 3.0. Consequently, the optimal length of piles is around $3.0R_L$ for the speed $c = 0.2v_{SH}$. For the case of $c = 0.5v_{SH}$ and $c = 0.7v_{SH}$, when the length of the pile L/λ_R is larger than 2.0, the influence of the length of piles becomes less. Thus, for these speeds, the optimal length of piles is around $2.0R_L$. Obviously, the Rayleigh wave accounts for the major part of the energy of the waves propagating near the surface of the half-space. It is well known that the Rayleigh wave is confined near the surface. Thus, if the pile bottoms are beyond the influence domain of the Rayleigh waves, the pile length will makes no difference on the vibration isolation effect of the pile row, which is consistent with the finding in Ref. [13].

5.5. *Effect of pile net spacing*

The net spacing (s) between neighboring piles in a pile row is an important parameter for the design of vibration isolation by pile rows. In this section, it is assumed that the parameters for the piles and the moving point load take the same values as those of Section 6.2, while value of pile net spacing s takes the values 0.5, 1.0 and 2.0 m, respectively. For each pile net spacing s, three different values of the load speed $c = 0.2v_{SH}$, $0.5v_{SH}$ and $= 0.7v_{SH}$, respectively, are considered where $v_{SH} = \sqrt{\mu/\rho}$.

Fig. 13(a)–(c) gives the variation of the amplitude reduction ratio A_r along $0 \leqslant x/R_L \leqslant 2$, $y = 0$ for $s = 0.5$, 1.0 and 2.0 m at the instant when the moving load is at the point $(x, y, z) = (-7.5, 0, 0\,\text{m})$ with velocity $c = 0.2v_{SH}$, $0.5v_{SH}$ and $= 0.7v_{SH}$, respectively. Fig. 14 plots the variation of the average amplitude reduction ratio $\bar{A}_r$ versus the pile net spacing s for the cases of the load speed $c = 0.2v_{SH}$, $0.5v_{SH}$ and $= 0.7v_{SH}$, respectively, when the moving load is located at the point $(x, y, z) = (-7.5, 0, 0\,\text{m})$.

Fig. 14 shows that the average amplitude reduction ratio $\bar{A}_r$ has appreciable increment when the net spacing s increases, which clearly shows that with increasing net spacing s, the vibration reduction effect of the pile row reduces considerably. Generally, smaller separation between piles will produce a better vibration reduction effect. Also, Fig. 14 illustrates that the influence of the net spacing on the vibration isolation effect for high-speed cases is more pronounced than that for lower speed cases.

6. Conclusions

The numerical simulation of the isolation of the vibration by pile rows has been carried out in this study. The semi-analytical nature of the proposed method avoids the discretization of the whole calculation domain,

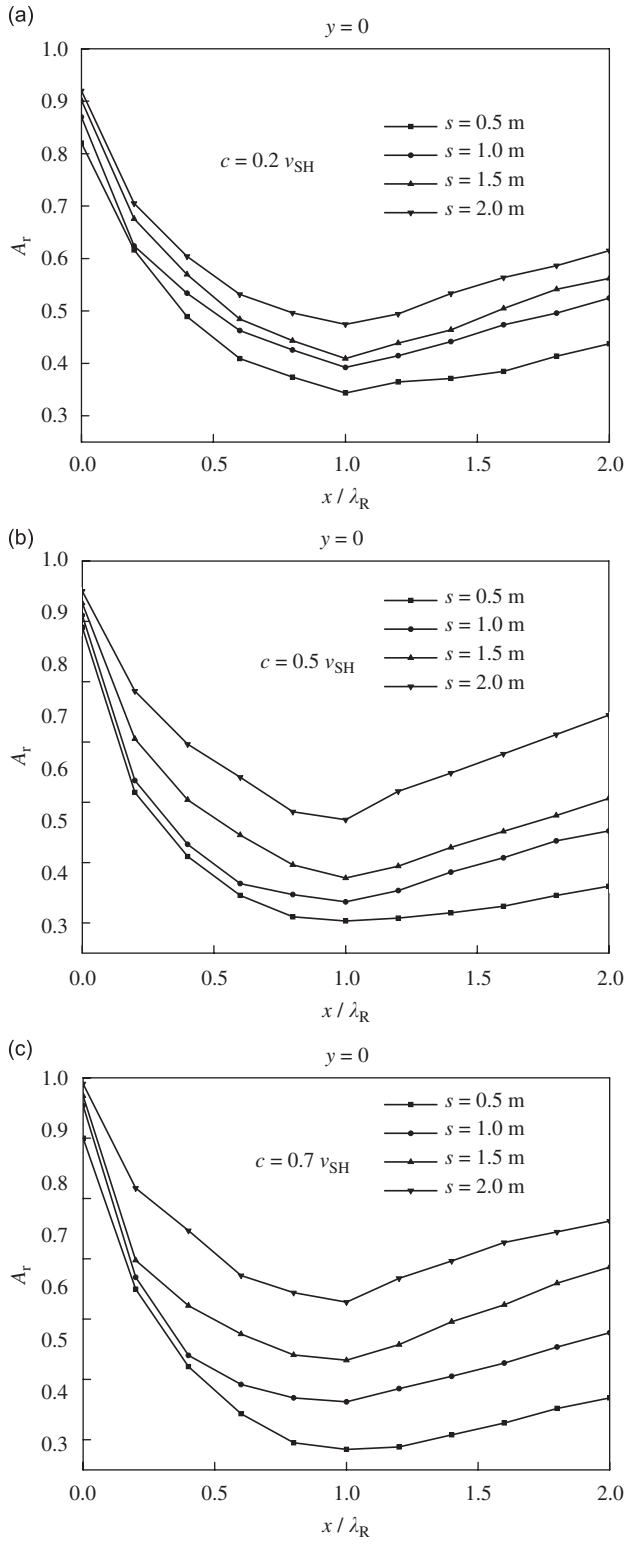

Fig. 13. The amplitude reduction ratio A_r within the range $0 \leqslant x/R_L \leqslant 2$ and $y = 0$ for different values of $s = 0.5$, 1.0, 1.5 and 2.0 m at the time when the moving load passing the point $(x, y, z) = (-7.5, 0, 0\,\text{m})$ with three velocities: (a) $c = 0.2 v_{SH}$; (b) $c = 0.5 v_{SH}$; (c) $c = 0.7 v_{SH}$.

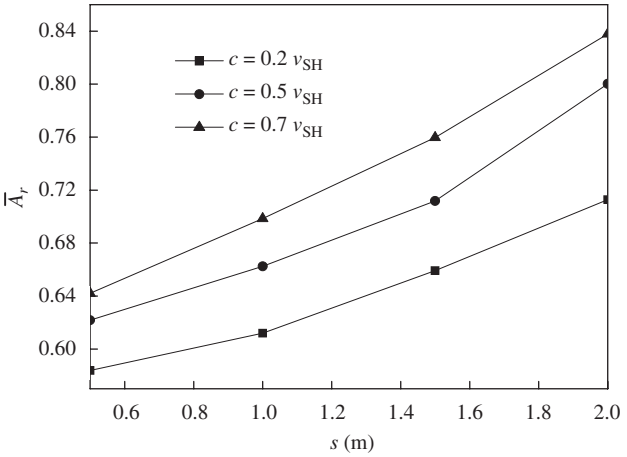

Fig. 14. The influence of pile net spacing s on the average amplitude reduction ratio $\bar{A}_r$ at the time for the moving load passing the point $(x, y, z) = (-7.5, 0, 0\,\text{m})$ with three different velocities $c = 0.2v_{SH}$, $0.5v_{SH}$ and $= 0.7v_{SH}$, respectively.

and thus it reduces the CPU time for the current problem substantially. Also, to verify the proposed method, results of this study were compared with known results. Numerical results show that our solution is in a good agreement with existing results.

To study the vibration isolation effect, the influences of the moving load speed, Young's modulus of the pile, the pile length and the spacing between piles have been investigated. Based on the numerical simulations performed in this study, following conclusions can be drawn:

(1) The same pile rows can achieve better vibration isolation effect for lower speed loads than for higher speed loads. Moreover, for the same pile rows and the vibration source, the poroelastic medium often leads to a better vibration isolation effect than the single-phase elastic medium does.
(2) Young's modulus of the pile is an important parameter affecting the vibration isolation effect. Increase of Young's modulus of the pile will enhance the vibration isolation effect.
(3) Pile length is also an important factor affecting the vibration isolation effect. Generally, the pile rows with longer pile length will have a better vibration isolation effect than those with shorter pile length. The optimal length of piles for high-speed loads is shorter than that for lower speed loads. For example, according to our calculations, the recommended optimal lengths for piles are $3.0\lambda_R$, $2.0\lambda_R$, for $c = 0.2v_{SH}$ and $0.7v_{SH}$, respectively, in which λ_R is the wavelength of the Rayleigh wave.
(4) The net spacing between neighboring piles is crucial for the vibration isolation effect. Generally, to obtain a better vibration isolation effect for high-speed loads, the net spacing should take smaller values.

Acknowledgments

This research is carried out in the framework of the project from the National Natural Science Foundation of China with Grant no. 50578071. Also, the research is supported by the returned oversea scholar funding from Chinese Education Ministry. Moreover, the financial support from Shanghai Leading Academic Discipline Project with Project no. B208 is greatly appreciated.

References

[1] K. Emad, G.D. Manolis, Shallow trenches and propagation of surface waves, *Journal of Engineering Mechanics—ASCE* 111 (1985) 279–282.
[2] D.E. Beskos, G. Dasgupta, I.G. Vardoulakis, Vibration isolation using open or filled trench—part 1: 2-D homogeneous, *Computational Mechanics* 1 (1986) 43–63.
[3] B. Dasgupta, D.E. Beskos, I.G. Vordouclakis, Vibration isolation using open or filled trenches—part 2: 3-D homogeneous soil, *Computational Mechanics* 6 (1990) 129–142.

[4] J. Avilles, F.J. Sanchez-Sesma, Foundation isolation from vibration using piles as barriers, *Journal of Engineering Mechanics—ASCE* 114 (1988) 1854–1870.
[5] S.E. Kattis, D. Polyzos, D.E. Beskos, Modelling of pile wave barriers by effective trenches and their screening effectiveness, *Soil Dynamics and Earthquake Engineering* 18 (1999) 1–10.
[6] S.E. Kattis, D. Polyzos, D.E. Beskos, Vibration isolation by a row of piles using a 3-D frequency domain BEM, *International Journal for Numerical Methods in Engineering* 46 (1999) 713–728.
[7] P.H. Tsai, Y.F. Zheng, T.L. Jen, Three-dimensional analysis of the screening effectiveness of hollow pile barriers for foundation-induced vertical vibration, *Computers and Geotechnics* 35 (2008) 489–499.
[8] M.A. Biot, Theory of propagation of elastic waves in a fluid-saturated porous solid. I. Low frequency range, *Journal of the Acoustical Society of America* 28 (1956) 168–178.
[9] M.A. Biot, Theory of propagation of elastic waves in a fluid-saturated porous solid. II: Higher frequency range, *Journal of the Acoustical Society of America* 28 (1956) 179–191.
[10] M.A. Biot, Mechanics of deformation and acoustic propagation in porous media, *Journal of Applied Psychology* 33 (1962) 1482–1498.
[11] X. Zeng, R.K.N.D. Rajapakse, Dynamic axial load transfer from elastic pile to poroelastic medium, *Journal of Engineering Mechanics* 125 (1999) 1048–1055.
[12] J.H. Wang, X.L. Zhou, J.F. Lu, Dynamic response of pile groups embedded in a poroelastic medium, *Soil Dynamics and Earthquake Engineering* 23 (2003) 235–242.
[13] B. Jin, Z. Zhong, Lateral dynamic compliance of pile embedded in poroelastic half space, *Soil Dynamic and Earthquake Engineering* 21 (2001) 519–525.
[14] R. Muki, E. Sternberg, On the diffusion of an axial load from an infinite cylindrical pile embedded in an elastic medium, *International Journal of Solids and Structures* 5 (1969) 587–606.
[15] R. Muki, E. Sternberg, Elastostatic load transfer to a half space from a partially embedded axially loaded rod, *International Journal of Solids and Structures* 6 (1970) 69–90.
[16] I.N. Sneddon, *Fourier Transforms*, McGraw-Hill, New York, NY, 1951.
[17] J.F. Lu, D.S. Jeng, A half-space saturated poro-elastic medium subjected to a moving point load, *International Journal of Solids and Structures* 44 (2007) 573–586.
[18] J.F. Lu, D.S. Jeng, W.D. Nie, Dynamic response of a pile embedded in a porous medium and subjected to plane SH waves, *Computers and Geotechnics* 33 (2006) 404–418.
[19] M.R. Halpern, P. Christiano, Steady-state harmonic response of a rigid plate bearing on a liquid-saturated poroelastic halfspace, *Earthquake Engineering and Structural Dynamics* 14 (1986) 439–454.
[20] R.Y. Pak, P.C. Jennings, Elastic dynamic response of pile under transverse excitations, *Journal of Engineering Mechanics Division—ASCE* 113 (1987) 1101–1116.
[21] R.D. Woods, Screening of surface waves in soil, *Journal of Soil Mechanics and Foundation Engineering—ASCE* 94 (SM4) (1968) 951–979.
[22] A.V. Oppenheim, R.W. Schafer, *Discrete-Time Signal Processing*, Prentice-Hall, Inc., Englewood Cliffs, NJ, 1999, pp. 514–580.
[23] J.M. Carcione, *Wave Fields in Real Media: Wave Propagation in Anisotropic, Anelastic, and Porous Media*, Pergamon, Amsterdam, 2001.